

**Set of holonomic and protected gates on topological qubits for a realistic quantum computer**Andrey R. Klots<sup>1</sup> and Lev B. Ioffe<sup>2,3</sup><sup>1</sup>*Department of Physics, University of Wisconsin–Madison, Madison, Wisconsin 53706, USA*<sup>2</sup>*Laboratory for Condensed Matter Physics, National Research University HSE, Myasnitskaya Strasse 20, Moscow 101978, Russia*<sup>3</sup>*Google Inc., Venice, California 90291, USA* (Received 13 May 2021; revised 2 August 2021; accepted 5 August 2021; published 6 October 2021)

In recent years qubit designs such as transmons have approached fidelities of up to 0.999. However, even these devices are still insufficient for realizing quantum error correction requiring better than 0.9999 fidelity. Topologically protected superconducting qubits are arguably the most prospective for building a realistic quantum computer as they are intrinsically protected from noise and leakage errors that occur in transmons. We propose a topologically protected qubit design based on a  $\pi$ -periodic Josephson element and a universal set of gates: A protected Clifford group and highly robust (with infidelity  $\lesssim 10^{-4}$ ) nondiscrete holonomic phase gate. The qubit is controlled via charge  $Q$  and flux  $\Phi$  biases. The holonomic gate is realized by quickly, but adiabatically, going along a particular closed path in the two-dimensional  $\{\Phi, Q\}$  space—a path where computational states are always degenerate but Berry curvature is localized inside the path. This gate is robust against currently achievable noise levels. This qubit architecture allows building a realistic scalable superconducting quantum computer with leakage and noise-induced errors below  $10^{-4}$ , which allows performing realistic error correction codes with currently available fabrication techniques.

DOI: [10.1103/PhysRevB.104.144502](https://doi.org/10.1103/PhysRevB.104.144502)**I. OVERVIEW**

The main challenge in building a realistic quantum computer is building a qubit and developing logical operations that can be used for efficient error corrections [1]. The problem with currently existing qubits is twofold. First, the best fidelity of the existing qubits is either insufficient for error correction or requires an impractically large hardware overhead. Second, the transmons displaying the best fidelity achieve it by reducing nonlinearity, increasing leakage out of computational space that is very difficult to correct within surface code [2–5]. With increasing complexity of the quantum algorithm, surface codes require a rapidly increasing number of physical qubits to perform error correction. As an alternative, it is desirable to create qubits that are protected against noise-induced bit-flip and phase errors on the hardware level. Arguably, the most prospective design involves using a  $\pi$ -periodic element [6–10], effectively a Josephson element that allows tunneling of only an even number of Cooper pairs and has the phase-energy ( $\varphi$ - $E$ ) relation  $E(\varphi) = -E_2 \cos 2\varphi$ , with  $E_2$  being the Josephson energy for double-Cooper-pair tunneling. Such an element coupled to a large capacitor  $C$  with charging energy  $E_C \ll E_2$  [here  $E_C = (2e)^2/2C$ ] forms the qubit [Fig. 1(a)] in which two logical states are characterized by the charge parity (i.e., the parity of the number of Cooper pairs) on the superconducting island: “0” and “1” logical states are encoded by even and odd charge states, respectively. The dephasing rate for such a qubit is exponentially suppressed with an increasing value of  $\sqrt{E_2/E_C}$ , which is a square of the characteristic width of the wave function  $\psi(n)$  in the

charge space  $n$ . In this respect, the  $\pi$ -periodic qubit is similar to the transmon, for which protection is achieved due to the exponential suppression of the energy dispersion as a function of the charge offset  $Q$ . However, unlike transmons,  $\pi$ -periodic qubits are strongly anharmonic and have nearly degenerate computational states well separated from excited ones, preventing leakage outside of the computational space. At the same time, bit flips in this protected qubit are exponentially suppressed due to an exponentially small value of a  $\cos \varphi$  term responsible for single-Cooper-pair tunneling.

Ideally, a protected qubit should allow a universal set of fault-tolerant operations during which the qubit remains protected. Here the term “protected” implies exponential suppression of any noise, and the term “robust” implies suppression of linear noise. In this paper we show that a relatively minor modification of the  $\pi$ -periodic qubit gives an almost ideal protected qubit. Namely, it allows a fault-tolerant (i.e., with exponentially small error)  $Z(\frac{\pi}{2})$  discrete Clifford phase gate and a robust nondiscrete (i.e., non-Clifford) holonomic phase gate  $Z(\Theta)$  along with the previously proposed [10]  $X(\frac{\pi}{2})$  and  $[X \otimes X](\frac{\pi}{2})$  gates. Note that the nondiscrete gate does not need to be exactly a  $\pi/8$  rotation. Altogether, these gates allow universal qubit control [11]. During all these operations the qubit states remain degenerate. While this degeneracy is exponentially protected during discrete gates, it is insensitive in the linear order only to the charge noise for the holonomic phase gate. Furthermore, due to degeneracy of the computational states the holonomic operation is not sensitive to a precise form of the pulse shape in the time domain and

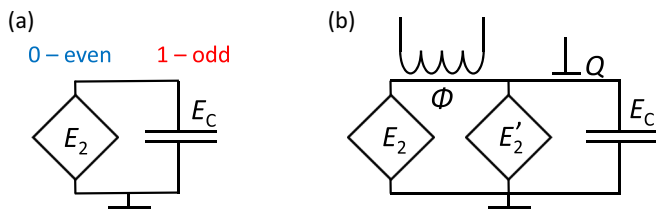


FIG. 1. Schematics of (a) the protected  $\pi$ -periodic qubit and (b) its modification that allows a full set of operations.

allows exponentially small Landau-Zener-type leakage out of the computational space. Because holonomic operations are robust but not exponentially protected, the resulting qubit is *almost ideal*.

The modification that gives an almost ideal qubit is the ability to vary the value of the Josephson energy  $E_2$  together with the offset charge  $Q$ . Thus, we control two parameters, and a closed path in the two-dimensional (2D) parameter space produces the Berry phase of the qubit. Variation of the effective  $E_2$  can be achieved by replacing a  $\pi$ -periodic element by a dc-SQUID-like loop (where SQUID indicates a superconducting quantum interference device) of two similar  $\pi$ -periodic elements connected in parallel [Fig. 1(b)]. We refer to this circuit as  $\pi$ -SQUID with effective Josephson energy  $E_2^{\text{eff}}$  depending on flux  $\Phi$  through the loop. For  $\Phi = 0$ , effective  $E_2^{\text{eff}}$  is the largest, and the qubit behaves like a regular protected  $0$ - $\pi$  qubit. Increasing  $\Phi$  decreases  $E_2^{\text{eff}}$ . When  $\sqrt{E_2^{\text{eff}}/E_C} \lesssim 1$  a relatively slow variation of the parameters (an estimate will be given below) squeezes the qubit wave function to only one or two charge states, and protection is lifted. This temporary removal of protection creates a strong charge  $Q$  dispersion and allows us to perform different phase gates.

We show below that flux and charge bias variables  $\{\Phi, Q\}$  form a 2D parameter space, in which the qubit possesses the Berry curvature shown in Fig. 2(a) that is obtained analytically. The Berry curvature has a strong peak at  $(\Phi = \Phi_0/4, Q = 0)$ . The nondiscrete phase gate is performed by

adiabatically going in a loop around this peak and gaining different Berry phases for the two logical states. It is crucial that one can choose the path so that at every point the computational states remain degenerate and Berry curvature is zero. The preservation of degeneracy implies that the gate is holonomic: Lifting protection does not cause a gain of the unwanted time-dependent dynamic phase. Furthermore, it provides exponential protection against flux noise, while the symmetric nature of the  $Q = 1/2$  point implies the absence of the linear response to charge noise. Throughout the paper we use units of  $\hbar = 2e = 1$  and  $\Phi_0 = 2\pi$ .

The protected Clifford  $Z(\frac{\pi}{2})$  phase gate is performed by turning the  $\pi$ -SQUID off, thereby allowing the qubit to evolve only under the quadratic capacitor Hamiltonian  $H_C = E_C n^2$ . Analogously to the  $X(\frac{\pi}{2})$  gate [10], by choosing the proper gate timing we can make even states gain zero dynamic phase and all odd states gain a dynamic phase of  $-\pi/2$ . Similar to the  $X(\frac{\pi}{2})$  gate, this transformation is protected, and the errors are flagged by the qubit excitation to a high-energy state.

## II. QUALITATIVE DESCRIPTION OF THE HOLONOMIC GATE

Figure 2(a) shows the path (dashed orange loop) along which the holonomic gate is performed. Red areas depict protected regions where  $\Phi$  is close to zero (or  $\pi$ ) and  $\sqrt{E_2^{\text{eff}}/E_C} \gg 1$ . Outside that region ( $\sqrt{E_2^{\text{eff}}/E_C} \lesssim 1$ ) the qubit is in an unprotected regime.

The loop can be split into two branches: Top ( $Q > 0$ ) and bottom ( $Q < 0$ ). First, we go along the  $Q > 0$  branch applying a positive charge bias on the superconducting island while keeping the qubit protected [Figs. 2(a) and 2(b), point 1]. Then, increasing the flux through the loop, we lift the protection against dephasing and squeeze the even wave function into only one charge state of  $n = 0$  and the odd wave function into  $n = 1$  (points 2 and 3). Importantly, the flux through the  $\pi$ -SQUID loop also creates a gauge transformation that rotates each charge state  $n$  on the island by a different phase factor  $n\tilde{\Phi}$ , where  $\tilde{\Phi}$  is some gauge-related rotation angle that

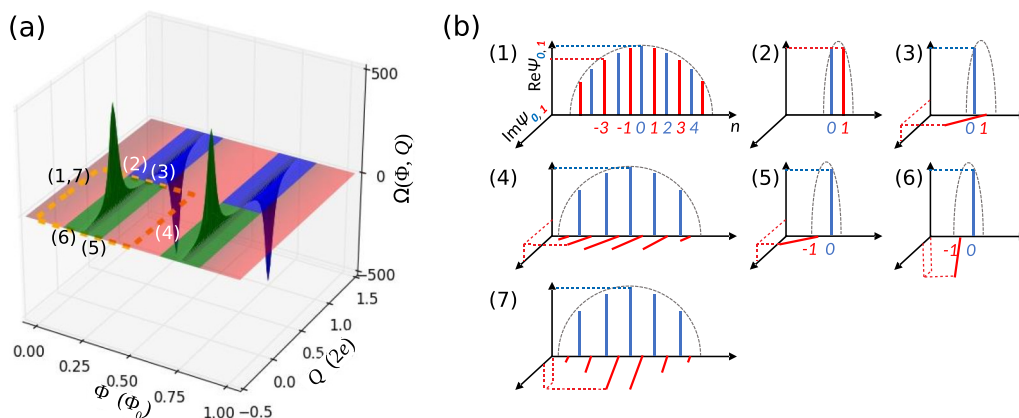


FIG. 2. Berry curvature and phase. (a) Berry curvature in parameter space  $\{\Phi, Q\}$ . The protected region is shown in red; the unprotected region is in green and blue. The holonomic transformation is achieved by changing the parameters along the dashed orange line that starts at point 1 in the protected regime. (b) Cartoons of the wave function at a few characteristic points in parameter space. Dashed lines show projections of wave functions onto the complex plane. Points 1, 4, and 7 correspond to protected regime; points 2, 3, 5, 6 correspond to the unprotected one (see text).

will be discussed and derived further. As a result, on the  $Q > 0$  branch the  $n = 0$  state remains unaffected, but the strongest odd state [Fig. 2(b), points 2 and 3]  $n = +1$  gains the phase of  $(+1)\tilde{\Phi}$ . Then we return to our initial state through the  $Q < 0$  branch [Fig. 2(b), points 4–7]. On this branch the gauge transform is performed in the opposite direction ( $\tilde{\Phi} \rightarrow -\tilde{\Phi}$ ). The dominant even state  $n = 0$  is again unaffected, but the odd state, now represented by the  $n = -1$  charge state, gains the phase of  $(-1)(-\tilde{\Phi})$ , which has the same sign as on the  $Q > 0$  branch. Thus, on both halves of the path the odd state is rotated in the same direction, causing a nondiscrete rotation that is smaller than  $\pi$  by a value proportional to the asymmetry of the  $\pi$ -SQUID.

### III. QUANTITATIVE DESCRIPTION OF THE HOLONOMIC GATE

First, let us discuss the properties of the Hamiltonian and its eigenfunctions. We focus on the designs of  $\pi$ -periodic elements in which computational energy levels are well separated from excited ones [6,7]. The energy of the  $\pi$ -SQUID is  $E(\varphi) = -E_2 \cos(\varphi - \Phi/2) - E'_2 \cos(\varphi + \Phi/2)$ . In this case the relevant low-energy degrees of freedom of the qubit are described by the Hamiltonian

$$\mathcal{H} = E_C(n - Q)^2 - E_2^{\text{eff}}(\Phi) \cos 2[\varphi - \tilde{\Phi}(\Phi)]. \quad (1)$$

Here

$$E_2^{\text{eff}}(\Phi) = \sqrt{E_2^2 + E_2'^2 + 2E_2E_2' \cos(2\Phi)}, \quad (2)$$

$$\tilde{\Phi}(\Phi) = \frac{1}{2} \arctan \left( \frac{\sin \Phi}{E_2 + E_2'}, \frac{\cos \Phi}{E_2' - E_2} \right), \quad (3)$$

with Josephson energies  $E_2$  and  $E_2'$  for the two  $\pi$ -periodic elements. We choose parameters so that  $E_2 + E_2' \gg E_C \gg |E_2 - E_2'|$ . This allows us to have both protected [ $E_2^{\text{eff}}(0)/E_C \gg 1$ ] and unprotected [ $E_2^{\text{eff}}(\pi/2)/E_C \ll 1$ ] regimes. The eigenfunctions  $\psi(n)$  of such a Hamiltonian are represented by either even or odd charge states enclosed by an envelope function with a width  $\sim (E_2^{\text{eff}}/E_C)^{1/4}$  that is centered around  $n = Q$  in the charge space [Fig. 2(b), points 1 and 2]. Note that for half-integer  $Q$  even and odd eigenstates have mirror symmetry, which means that for half-integer  $Q$  computational states are degenerate regardless of  $\Phi$ . Thus, the offset charge  $Q$  changes the balance between even and odd states. Flux bias, in turn, changes the width of the wave function by modifying  $E_2^{\text{eff}}$ . However, flux bias has another crucial effect: Although it is tempting to disregard the phase offset  $\tilde{\Phi}$  in (1), it should not be done because in our gate  $\tilde{\Phi}$  is a function of  $\Phi$ , which is not constant. In fact, this term plays a key role in realizing the gate: Since the potential in (1) is shifted by  $\tilde{\Phi}$  in the  $\varphi$  space, the wave function  $\psi(\varphi)$  is also transformed as  $\psi(\varphi) \rightarrow \psi(\varphi - \tilde{\Phi})$ . In the charge space this results in a gauge transformation  $\psi(n) \rightarrow \exp(in\tilde{\Phi})\psi(n)$ , as mentioned in the previous section.

### IV. CALCULATING BERRY CURVATURE

The phase accrued by the computational states when going along the loop is calculated as an integral of the Berry curvature

over the area enclosed by the loop. In this section we derive the expression for the Berry curvature.

We begin with the region of  $\Phi \approx \pi/2$ , where  $E_2^{\text{eff}} \lesssim E_C$  and the computational eigenfunctions are squeezed to only one or two charge states (Fig. 2, point 2). For any value of  $Q$  it is convenient to write the effective Hamiltonian in terms of the two charge states  $n$  nearest to  $Q$ . For example, for  $0 < Q < 1$  the odd state can be written in the basis of two wave functions  $\psi_{\pm 1}(\varphi) = (2\pi)^{-1/2} \exp(\pm i\varphi)$ , corresponding to  $n = \pm 1$  charge states, while relevant even states are  $\psi_0(\varphi) = (2\pi)^{-1/2}$  and  $\psi_2(\varphi) = (2\pi)^{-1/2} \exp(2i\varphi)$ :

$$\mathcal{H}_{\text{eff}}^{\text{odd}} \approx -\frac{1}{2}E_2^{\text{eff}}(\sigma^x \cos 2\tilde{\Phi} + \sigma^y \sin 2\tilde{\Phi}) + QE_C\sigma^z, \quad (4)$$

$$\mathcal{H}_{\text{eff}}^{\text{even}} \approx -\frac{1}{2}E_2^{\text{eff}}(\sigma^x \cos 2\tilde{\Phi} + \sigma^y \sin 2\tilde{\Phi}) + (1 - Q)E_C\sigma^z. \quad (5)$$

Here  $\sigma^{x,y,z}$  are Pauli matrices in the space of  $|+1\rangle, |-1\rangle$  charge state vectors in (4) and in the basis of  $|0\rangle, |2\rangle$  in (5). The ground states of  $\mathcal{H}_{\text{eff}}^{\text{even}}$  and  $\mathcal{H}_{\text{eff}}^{\text{odd}}$  represent even and odd computational states, respectively. Note that such splitting of the Hamiltonian into two subspaces is possible due to an exponentially small  $\cos \varphi$  component of the potential of a well-fabricated protected  $0-\pi$  element. Higher eigenstates of  $\mathcal{H}_{\text{eff}}^{\text{odd(even)}}$  lie outside of the computational space. For the path shown in Fig. 2(a) the excited states always remain separated from the computational states by a large energy gap, so the effect of these excited states can be ignored. For  $-\frac{1}{2} \lesssim Q \lesssim \frac{1}{2}$  the accumulated phase is due to only odd eigenstates. To avoid the excitations of the higher-energy states of  $\mathcal{H}_{\text{eff}}^{\text{odd(even)}}$  the gate speed needs to be much slower than the smallest energy gap between the eigenvalues of  $\mathcal{H}_{\text{eff}}^{\text{odd(even)}}$  on the path, i.e.,

$$\tau_{\text{gate}}^{-1} \ll E_C, \quad (6)$$

where  $\tau_{\text{gate}}$  is the characteristic time of the gate operation. In the vicinity of a point  $\Phi \approx \pi/2$ ,  $Q = 1/2$ , Hamiltonians (4) and (5) assume a simple Landau-Zener form:

$$\mathcal{H}_{\text{eff}}^{\text{odd/even}} \approx -\frac{E_2 + E_2'}{2} \sigma^x \left( \Phi - \frac{\pi}{2} \right) + \frac{|E_2 - E_2'|}{2} \sigma^y + \frac{E_C}{2} \sigma^z. \quad (7)$$

Analytically, assuming  $|E_2 - E_2'| \ll E_C$ , the probability of Landau-Zener tunneling from the even (odd) computational state to the even (odd) excited state can be evaluated from the Hamiltonians (4), (5), and (7) as [12,13]

$$P = \exp \left[ -\tau_{\text{gate}} E_C^2 / (E_2 + E_2') \right]. \quad (8)$$

The ground state of (4) is described by a spinor,  $|\text{spinor}\rangle = (e^{-i\xi/2} \cos \theta/2, e^{+i\xi/2} \sin \theta/2)^T$ . Polar and azimuthal angles of the spinor are related to the qubit parameters as

$$\begin{aligned} \xi &= 2\tilde{\Phi}(\Phi), \\ \theta &= \arctan \left( -\frac{E_2^{\text{eff}}(\Phi)}{2}, E_C Q \right). \end{aligned} \quad (9)$$

In order to obtain the Berry curvature we perform a coordinate transform [ $\Phi = \Phi(\xi), Q = Q(\theta, \xi)$ ] and map the well-known Berry curvature of a spin  $\Omega_{\xi\theta}^{\text{spin}} = (1/2) \sin \theta$  onto variables  $(\Phi, Q)$  as  $\Omega_{\Phi Q}^{\text{eff}} = \frac{\partial \xi}{\partial \Phi} \frac{\partial \theta}{\partial Q} \Omega_{\xi\theta}^{\text{spin}}$ . Since  $\frac{\partial \tilde{\Phi}}{\partial \Phi}$  and  $\frac{\partial \xi}{\partial \Phi}$  have

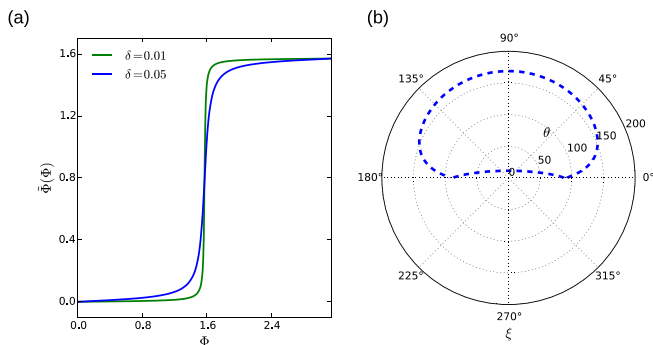


FIG. 3. Coordinate transformations. (a) Mapping of  $\Phi$  onto  $\tilde{\Phi}$  for  $\delta = 0.01, 0.05$ . (b) Coordinate transformation that relates the loop in the qubit parameter space  $\Phi$  and  $Q$  to the effective field acting on the spin, characterized by Euler angles  $\xi$  and  $\theta$ : Mapping of our loop onto the Bloch sphere.

a maximum at  $\Phi = \pi/2$  [Fig. 3(a)], most of the Berry curvature is concentrated in the vicinity of half-integer values of  $\Phi/\pi$ . This allows us write equations in the vicinity of  $\Phi = \Phi_0/4 = \pi/2$ . Let us introduce the new notations  $\alpha \stackrel{\text{def}}{=} \Phi - \pi/2$ ,  $E_\Sigma \stackrel{\text{def}}{=} E_2 + E_2'$ ,  $\delta \stackrel{\text{def}}{=} |E_2' - E_2|/E_\Sigma$ , and  $e_C \stackrel{\text{def}}{=} 2E_C/E_\Sigma$ . For large  $\alpha \gg e_C$  Eqs. (4) and (5) break down, but this regime gives little contribution to the Berry phase because in it the Berry curvature, along with the qubit charge dispersion, is exponentially suppressed with  $(\alpha/e_C)^{1/2}$ .

The dimensionless parameter that controls the Berry phase accumulated in the adiabatic evolution is

$$\eta = \delta/e_C = |E_2' - E_2|/2E_C.$$

In the following we assume that  $\eta \ll 1$ . The protection is removed when  $\alpha \lesssim e_C \ll 1$  and restored when  $\alpha \gg e_C$ . In the former regime the adiabatic evolution leads to accumulation of significant Berry phase. From (2) we approximate  $E_2^{\text{eff}}(\alpha) \approx E_\Sigma \sqrt{\delta^2 + \alpha^2}$ , and Berry curvature for the Hamiltonian (4) reduces to a simple form:

$$\Omega_{\Phi Q}^{\text{peak}}\left(\frac{\pi}{2} + \alpha, Q\right) = \frac{e_C}{2} \frac{\delta}{(\delta^2 + \alpha^2 + (e_C Q)^2)^{3/2}} \{1 + \mathcal{O}(\alpha^2)\}. \quad (10)$$

The total Berry curvature (the difference between  $\Omega_{\Phi Q}^{\text{peak}}$  for even and odd states) that determines the phase difference gained between odd and even states can be evaluated as

$$\Omega_{\Phi Q}(\Phi, Q) = \begin{cases} \Omega_{\Phi Q}^{\text{peak}}(\Phi, Q) - \Omega_{\Phi Q}^{\text{peak}}(\Phi, Q - 1), & Q > 0, \\ \Omega_{\Phi Q}^{\text{peak}}(\Phi, Q) - \Omega_{\Phi Q}^{\text{peak}}(\Phi, Q + 1), & Q < 0. \end{cases} \quad (11)$$

Since  $\Omega_{\Phi Q}$  is an odd function of  $Q - 1/2$ , it is equal to zero at half-integer values of  $Q$ . This expression holds for  $|Q| \leq 1/2$  and  $0 \leq \Phi \leq \pi$  but can be generalized to the entire  $\{\Phi, Q\}$  space by keeping in mind that  $\Omega_{\Phi Q}$  has a period of  $\pi$  in  $\Phi$  and a period of 2 in  $Q$ . Also, at half-integer values of  $Q$  the computational states are degenerate. Additionally, as mentioned above, the Berry curvature and energy splitting between the two lowest states are exponentially suppressed for  $\Phi \approx 0$  and  $\Phi \approx \pi$ . Thus, we choose our holonomic adiabatic path to go through these regions of  $\Phi = 0, \pi$  and  $Q = \pm 1/2$ .

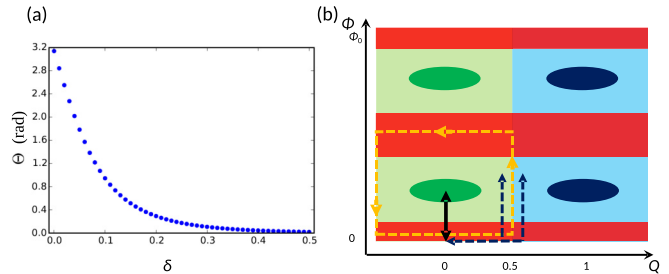


FIG. 4. Phase gates. (a) Phase  $\Theta$  as a function of the  $\pi$ -SQUID asymmetry  $\delta$  assuming  $e_C = 0.1$ . (b) Sketch of the Berry curvature map with a depiction of paths that realize different gates. Orange dashed line: Rectangular adiabatic loop to realize the holonomic phase gate. Black solid line: Quick diabatic  $X(\pi/2)$  gate realized by quick frustration of the  $\pi$ -SQUID. Dark-blue dashed line: Example of an idle gate that can be used in CPMG or multiple echo sequences. During the idle gate only accrual of the positive or negative noise-induced dynamic phase occurs. This can be used to create a multiple charge-echo effect to partially compensate the random dynamic phase accrued during the holonomic gate.

## V. BERRY PHASE

Let us evaluate the Berry phase that is given by the integral of the Berry curvature (10) over  $\alpha$  and  $Q$  in the leading approximation in  $\eta \ll 1$ . The integral is dominated by the region  $\{|\alpha| \lesssim \delta, |e_C Q| \lesssim \delta\}$ . For  $\delta \ll e_C$  this implies that  $\alpha \ll e_C$ ,  $Q \ll 1$ , which justifies the use of (10). If we were to integrate the curvature (10) in the infinite limits of  $\alpha$  and  $Q$ , we would get  $\Theta_0 = \pi$  for the Berry phase. However, exponential suppression of curvature for  $\alpha > e_C$  and the finite size of the loop limited by  $Q \approx \pm 1/2$  imply that the actual Berry phase is given by the integral that is cut off in these directions:

$$\begin{aligned} \Theta &\approx \int_{\sim -e_C}^{\sim e_C} d\alpha \int_{\sim -e_C/2}^{\sim e_C/2} d(e_C Q) \frac{\delta/2}{[\delta^2 + \alpha^2 + (e_C Q)^2]^{3/2}} \\ &\approx \pi - \mathcal{A} \frac{\delta}{e_C}, \end{aligned} \quad (12)$$

giving us the leading approximation in  $\eta = \delta/e_C$ . This simple analytical computation does not give the value of the constant  $\mathcal{A} \sim 1$  which we determined numerically. Simple analytical estimates provided above can be easily performed in the limit of  $\delta \ll e_C \ll 1$ . However, for the other parameter regime of  $\delta \sim e_C$  the gate will still work, but the rotation angle needs to be calculated numerically. We performed such numerical calculations [see Fig. 4(a)] to verify the predicted behavior of the gate. Our numerical calculations done by diagonalizing the Hamiltonian (1) in the basis of the 201 charge-state wave vector  $\{|-100\rangle, |-99\rangle, \dots, |100\rangle\}$  and going along the contour with a step of  $0.001\pi$  in  $\Phi$  and 0.01 in  $Q$  determine the numerical constant  $\mathcal{A} = 2.97 \pm 0.02$ . While (12) works for small  $\delta$ ,  $e_C$ , and  $\eta$ , numerical simulations work for any parameter range and match (12) in this small-parameter regime.

Most importantly, the resulting phase rotation is non-Clifford: It deviates from a rotation of  $\pi$  by a value that can be controlled by tuning the qubit design. For reasonably achievable values of  $\delta \sim 10^{-2}$  and  $e_C \sim 10^{-1}$ ,  $\eta \sim 0.1$ , and the non-Clifford rotation is  $\mathcal{A}\eta \sim 0.3$  rad. A value of  $\eta \simeq 0.1$  gives a rotation  $\Theta \simeq \pi - \pi/8$ , which is a desired  $\pi/8$  rotation

modulo a Clifford rotation. However, non- $\pi/8$  rotations also allow for universal quantum computing. The non-Clifford nature of this gate can be understood by mapping the rectangular path in the  $\{\Phi, Q\}$  space onto a Bloch sphere  $\{\xi, \theta\}$  using Eqs. (9). As shown in Fig. 3(b), the path covers an area which is somewhat less than half of the Bloch sphere. Moreover, our numerical modeling shows that further increasing of  $\eta$  can yield any phase [Fig. 4(a)] from  $\Theta \approx \pi$  for  $\eta \ll 1$  to  $\Theta \rightarrow 0$  for  $\eta \gtrsim 1$ , the regime when the qubit does not leave the protected state [ $E_2^{\text{eff}}(\nabla\Phi) \gg E_C$ ] and  $\Omega_{\Phi Q}$  remains exponentially small. Although the analytical derivations above provide some intuition for understanding the gate in the  $\delta \ll e_C$  regime, numerical simulations show that the gate also provides a significant phase rotation of  $\Theta \sim 0.1$  rad for  $\eta = \delta/e_C$  up to  $\eta \sim 3$ . In practice it is easier to controllably fabricate devices with larger asymmetry  $\delta$ .

## VI. GATE ERRORS AND TIMING

Since the part of the path sensitive to the flux noise ( $\Phi \approx 0, \pi; -\frac{1}{2} \leq Q \leq \frac{1}{2}$ ) is located in the protected regime of  $E_2^{\text{eff}}/E_C \gg 1$ , the effects of the flux noise are exponentially suppressed. In order to estimate the effect of the low-frequency charge noise, assume that the horizontal (i.e., in the  $\Phi$  direction) part of the path is shifted vertically by a small value  $\epsilon_Q$ , so that  $Q = 1/2 + \epsilon_Q$  instead of  $Q = 1/2$ . This path would give a Berry phase that differs from (12) by

$$\begin{aligned} \Delta\Theta &\sim \int_{\sim -\epsilon_C}^{\sim +\epsilon_C} d\alpha \int d\epsilon_Q \Omega_{\Phi Q} \left( \frac{\pi}{2} + \alpha, \frac{1}{2} + \epsilon_Q \right) \\ &\sim \int \eta \epsilon_Q d\epsilon_Q \sim \eta \epsilon_Q^2. \end{aligned} \quad (13)$$

Here we used the fact that  $\Omega_{\Phi Q} \sim \eta \epsilon_Q$  is linear with  $\epsilon_Q$  near  $Q = \pm 1/2$ . Thus, from (12) the relative error of the non-Clifford part ( $\Theta \bmod \pi$ ) of the phase rotation  $\Theta$  is  $\epsilon_{\Theta}^{\text{rel}} \sim \Delta\Theta/\eta \sim \epsilon_Q^2$ . Assuming a high value of the charge noise  $\epsilon_Q \sim 10^{-2}$  on few-second timescales [14–17], we arrive at a relative gate error as low as  $\epsilon_{\Theta}^{\text{rel}} \sim 10^{-4}$ , yielding a very small infidelity.

In order for the gate to be considered adiabatic to a reasonable degree, we want to have the previously estimated probability of Landau-Zener tunneling (8) out of the computational space to be  $P = \exp[-\tau_{\text{gate}} e_C^2 E_{\Sigma}/4] \sim 10^{-4}$ . For reasonable values  $e_C \sim 10^{-1}$  and  $E_{\Sigma} \sim 2\pi \times 40$  GHz [6], we get the gate timing  $\tau_{\text{gate}} \gtrsim 15$  ns.

Finally, we consider the strongest source of error due to accumulation of an unwanted dynamic phase. We consider this to be the bottleneck problem for any protected qubit design because in order to perform a non-Clifford rotation one needs to temporarily remove the protection by either (a) lifting the degeneracy of the computational states, which leads to error linear with error in gate timing, or (b) keeping the degeneracy of the computational states (like in our case) at a cost of gaining linear dispersion of the computational states, which leads to error linear in noise amplitude. In our gate, for example, the qubit remains in the unprotected regime  $\{\Phi \approx \frac{\pi}{2} \pm e_C, Q = \pm \frac{1}{2}\}$  during the time  $\tau_u \sim e_C \tau_{\text{gate}}$ , when it gains dynamic phase  $\gamma$ . There the computational states are degenerate, but their charge dispersion  $\Delta E_{1,0}(\epsilon_Q)$  is linear with

TABLE I. Gate infidelities due to charge-induced dynamic phase error. The values were obtained via numerical simulations with the following parameters: A basis of 201 charge states (as before), charge and flux steps of  $\Delta Q = 0.01$  and  $\Delta\Phi = 0.001\pi$ , and qubit energy scale  $E_{\Sigma} = 2\pi \times 40$  GHz. For each parameter set we run 10 trials using a  $1/f$  random function  $\epsilon_Q(t)$  with amplitude  $A^{1/2}$ , calculate the dynamic phase  $\gamma = \int_0^{2\tau_{\text{gate}}} \Delta E_{1,0}[\epsilon_Q(t)] dt$ , with  $dt = 9.1 \times 10^{-4} \tau_{\text{gate}}$ , and obtain an average deviation value  $\overline{\gamma^2}$ . The characteristic gate timing is  $\tau_{\text{gate}} = 15$  ns for  $e_C = 0.1$  and  $\tau_{\text{gate}} = (0.1/0.05)^2 \times 15 = 60$  ns for  $e_C = 0.05$  in order to satisfy the adiabaticity condition (8). Simulation results in the form  $(1-F)_{\text{min}} \sim (1-F)_{\text{max}}$  for the range of experimentally reported values of  $A^{1/2} = (1.5 \sim 6.5) \times 10^{-4}$  are shown.

	$1-F = \overline{\gamma^2}/2 (\times 10^{-6})$		
	$\delta = 0.01$	$\delta = 0.05$	$\delta = 0.1$
$e_C = 0.10$	1.3~26	1.0~19	0.50~9.5
$e_C = 0.05$	2.6~48	0.97~18	0.18~3.3

deviation  $\epsilon_Q$  of charge offset from  $Q = \pm 0.5$ . At  $\Phi = \pi/2$  the dispersion is  $\Delta E_{1,0}(\epsilon_Q) = \text{sgn}(Q) E_{\Sigma} e_C \epsilon_Q$ . Notably, for the  $Q > 0$  and  $Q < 0$  parts of the path the dynamic phase has opposite signs. Such accumulation of dynamic phase is identical to charge-echo experiments [15, 18, 19], which are sensitive to only high-frequency ( $f \gtrsim \tau_u^{-1}$ ) noise. Approximating the “turn-on” function for the unprotected regime as a square pulse, we can characterize the dynamic phase by its mean square using a well-known expression [18, 19]:

$$\overline{\gamma^2} \sim \int d\omega \Delta E_{1,0}^2 \frac{A}{\omega} \left( \frac{\sin(\omega\tau_u/2)}{\omega/2} \right)^2 \sim A(\Delta E_{1,0} \tau_u)^2.$$

Here  $A/\omega$  is the spectral density of  $1/f$  noise. We can now estimate the infidelity of the phase gate. Assume that the ideal gate acting on the initial qubit state  $|\text{initial}\rangle$  gives the state  $|\text{ideal}\rangle = Z(\Theta)|\text{initial}\rangle$ . The physical gate gives instead a state  $|\text{real}\rangle = Z(\Theta + \gamma)|\text{initial}\rangle$  with  $\gamma \ll 1$ . Define the mean infidelity as  $1-F = 1 - |\langle \text{ideal} | \text{real} \rangle| \approx \overline{\gamma^2}/2$ . Assuming the same parameters as above,  $E_{\Sigma} \sim 2\pi \times 40$  GHz,  $e_C = 0.1$ ,  $\tau_{\text{gate}} = 15$  ns, and high-frequency  $1/f$  charge noise with amplitude  $\epsilon_Q = A^{1/2}$  between  $1.5 \times 10^{-4} \times (2e)$  and  $6.5 \times 10^{-4} \times (2e)$  [15, 18, 20, 21], we get  $1-F$  between  $\sim 10^{-4}$  and  $\sim 10^{-5}$ . This estimate relies on the assumption that charge noise follows  $1/f$  dependence up to gigahertz frequencies, similar to the charge-sensitive devices studied in works by Astafiev *et al.* [15] and expected theoretically by Faoro and Ioffe [22]. In order to verify the estimated values of the charge-induced dynamic phase errors we used the aforementioned numeric model to calculate the dynamic phase contribution due to the effects of the charge noise for different qubit parameters. The flux and charge offsets are varied with time  $t$  as  $(\Phi(t), Q(t) + \epsilon_Q(t))$ , where  $\{\Phi(t), Q(t)\}$  go along the original ideal square loop shown in Fig. 4(b). Table I gives the simulated gate infidelities.

Compared to our conservative analytical estimate, the numerical results suggest infidelities that are on the low side with  $1-F < 10^{-5}$ . Note that once again, we see that higher  $\delta$  and lower  $e_C$  are preferable. For example, a realistic parameter set  $\delta = 0.1$ ,  $e_C = 0.05$  with  $\eta = 2$  yields rotation angle  $\Theta \approx \pi/12.5$  with infidelity  $\sim 10^{-6}$ .

In the regime of  $\eta \sim 2$  the dephasing can also be reduced by shortening the gate timing: In this regime, the Landau-Zener gap in (7) becomes bigger due to the larger  $\sigma^y$  component. The dephasing can be decreased even further by controlling the qubit using Gradient Ascent Pulse Engineering (GRAPE) [23] pulses to further minimize gate timing and by using Carr-Purcell-Meiboom-Gill (CPMG)-like [24] or multiple-echo sequences to filter out  $1/f$  noise [Fig. 4(b)]. This would give us further improvement in fidelity. This gate performance appears to be much better than in any currently existing qubit [25–27], especially considering a complexity of non-Clifford gates.

## VII. FAULT-TOLERANT CLIFFORD $Z(\pi/2)$ GATE

The proposed qubit can also be used to perform a protected Clifford  $\exp(-i\pi\sigma^z/4)$  gate. The idea is similar to the gate proposed in work by Brooks *et al.* [10]. In contrast to our non-Clifford gate, this gate is not performed adiabatically, but by quick modification of the Hamiltonian. While the adiabatic change of  $\Phi$  leads to squeezing of the wave function in the charge space, in the case of the quick modification of the Hamiltonian, the wave function does not have time to squeeze and remains as it was, delocalized in the charge space. In more detail, we start with the qubit in the protected state with  $\Phi = 0$  and  $E_2^{\text{eff}} = E_\Sigma$ . Then we quickly change the flux to  $\Phi = \pi/2$ . For  $\delta \ll e_C$ , this effectively turns off the  $\pi$ -SQUID, leaving only the capacitive part of the Hamiltonian  $\mathcal{H}(\pi/2) = n^2/2C + \mathcal{O}(\delta E_\Sigma \cos 2\varphi)$ , and hence, the qubit evolves under the operator  $U_{\pi/2}(t) \approx \exp\{-in^2(2C)^{-1}t\}$ . After time  $T = \pi C$  the qubit is brought back into the initial state. With this gate timing  $U_{\pi/2}(T) \approx \exp\{-i\pi n^2/2\}$ . As a result, all even charge states are multiplied by a factor of  $\exp\{-i\pi n_{\text{even}}^2/2\} = 1$ , and odd states are multiplied by  $\exp\{-i\pi n_{\text{odd}}^2/2\} = -i$ . Hence, we realize an  $\exp(-i\pi\sigma^z/4)$  gate. This gate is dual to the gate proposed in the work by Brooks *et al.* [10] and therefore has similar exponential stability against gate timing error  $T \rightarrow \pi C + \Delta T$  (see Sec. VI of [10]) and perturbation stability (e.g., against small perturbation  $\mathcal{O}(\delta E_\Sigma \cos 2\varphi)$  in the Hamiltonian; see Sec. XI of the work by Brooks *et al.* [10]).

Since in a protected state ( $\Phi = 0$ ) our qubit is identical to a standard  $0-\pi$  qubit [9,10] it is also possible to implement the  $\exp(i\pi\sigma^x/4)$  gate described by Brooks *et al.* [10]. With these two discrete gates it is possible to realize the topologically protected Clifford group  $\mathcal{C}_1$  and a two-qubit gate [10]  $\exp(i\pi X \otimes X/4)$ . In combination with the semiprotected holonomic gate described above it results in universal qubit control [11] with high fidelity.

## VIII. CONCLUSION

We showed that by adding one more degree of freedom to the protected qubit architecture based on double periodic Josephson junctions it is possible to realize two more types of gates: A discrete protected gate and a robust continuous holonomic gate that is not sensitive to the flux noise or to charge noise in the linear order. Together with previously existing one- and two-qubit flip gates [10] it is possible to build a realistic scalable quantum computer with universal qubit control and infidelity of the order of  $<10^{-4}$ /gate (importantly, with potential for further improvement). Similar to existing gates for  $0-\pi$  qubits[28] our scheme also requires temporary lifting of the protection. However, it also has two significant differences: (a) our gate can be implemented with only local on-chip bias lines without the need for RF pulses requiring additional cables and without the danger of frequency crowding; (b) since our gate is holonomic, we always stay inside the computational space with exponentially small probability of leakage, and keeping computational states nearly degenerate makes the gate robust against errors in pulse timing and shape. The time independence of the gate provides room for further gate optimization using optimized GRAPE pulses. The ability to have exponentially small leakage (8) is crucial as leakage errors are exceptionally harmful for fault-tolerant computing [2–5].

For the holonomic gate, in principle, one can also choose a different, more complicated path in the  $\{\Phi, Q\}$  space and achieve different phase gates with different noise sensitivities. This diversity arises due to the nontrivial Berry curvature landscape of an essentially two-dimensional system that is controlled by two bias channels. We expect that by creating more complex circuits with more degrees of freedom one can create systems with more complex Berry curvature landscapes and gauge fields. In the future it will be interesting to generalize this approach to other types of protected or robust qubits such as fluxonium [29–31]. We hope that further development of similar holonomic qubit architectures will allow achieving higher degrees of protection for continuous gates.

## ACKNOWLEDGMENTS

We thank R. F. McDermott, L. Faoro, and B. Christensen from the University of Wisconsin–Madison for useful discussions and comments. This work is supported by the U.S. Government under Grant No. ARO HiPS W911NF-18-1-0106.

- [1] R. Versluis, S. Poletto, N. Khammassi, B. Tarasinski, N. Haider, D. J. Michalak, A. Bruno, K. Bertels, and L. DiCarlo, Scalable quantum circuit and control for a superconducting surface code, *Phys. Rev. Appl.* **8**, 034021 (2017).  
 [2] P. Aliferis and B. M. Terhal, Fault-tolerant quantum computation for local leakage faults, *Quantum Inf. Comput.* **7**, 139 (2007).

- [3] N. C. Brown, A. Cross, and K. R. Brown, Critical faults of leakage errors on the surface code, in *2020 IEEE International Conference on Quantum Computing and Engineering (QCE)* (Denver, CO, USA, 2020), pp. 286–294.  
 [4] A. G. Fowler, Coping with qubit leakage in topological codes, *Phys. Rev. A* **88**, 042308 (2013).

- [5] M. Suchara, A. W. Cross, and J. M. Gambetta, Leakage suppression in the toric code, in *2015 IEEE International Symposium on Information Theory (ISIT)* (Hong Kong, China, 2015), pp. 1119–1123.
- [6] M. T. Bell, J. Paramanandam, L. B. Ioffe, and M. E. Gershenson, Protected Josephson Rhombus Chains, *Phys. Rev. Lett.* **112**, 167001 (2014).
- [7] S. Gladchenko, D. Olaya, E. Dupont-Ferrier, B. Douçot, L. B. Ioffe, and M. E. Gershenson, Superconducting nanocircuits for topologically protected qubits, *Nat. Phys.* **5**, 48 (2009).
- [8] L. B. Ioffe and M. V. Feigel'man, Possible realization of an ideal quantum computer in Josephson junction array, *Phys. Rev. B* **66**, 224503 (2002).
- [9] P. Groszkowski, A. Di Paolo, A. Grimsmo, A. Blais, D. Schuster, A. Houck, and J. Koch, Coherence properties of the  $0-\pi$  qubit, *New J. Phys.* **20**, 043053 (2018).
- [10] P. Brooks, A. Kitaev, and J. Preskill, Protected gates for superconducting qubits, *Phys. Rev. A* **87**, 052306 (2013).
- [11] S. Bravyi and A. Kitaev, Universal quantum computation with ideal Clifford gates and noisy ancillas, *Phys. Rev. A* **71**, 022316 (2005).
- [12] A. Shytov, D. Ivanov, and M. Feigel'man, Landau-Zener interferometry for qubits, *Eur. Phys. J. B* **36**, 263 (2003).
- [13] C. Zener, Non-adiabatic crossing of energy levels, *Proc. R. Soc. London, Ser. A* **137**, 696 (1932).
- [14] B. G. Christensen, C. D. Wilen, A. Opremcak, J. Nelson, F. Schlenker, C. H. Zimonick, L. B. Faoro, L. B. Ioffe, Y. J. Rosen, J. L. DuBois, B. L. T. Plourde, and R. McDermott, Anomalous charge noise in superconducting qubits, *Phys. Rev. B* **100**, 140503(R) (2019).
- [15] O. Astafiev, Y. A. Pashkin, Y. Nakamura, T. Yamamoto, and J.-S. Tsai, Quantum Noise in the Josephson Charge Qubit, *Phys. Rev. Lett.* **93**, 267007 (2004).
- [16] O. Astafiev, Y. A. Pashkin, Y. Nakamura, T. Yamamoto, and J.-S. Tsai, Temperature Square Dependence of the Low Frequency  $1/f$  Charge Noise in the Josephson Junction Qubits, *Phys. Rev. Lett.* **96**, 137001 (2006).
- [17] T. Henning, B. Starmark, T. Claeson, and P. Delsing, Bias and temperature dependence of the noise in a single electron transistor, *Eur. Phys. J. B* **8**, 627 (1999).
- [18] Y. Nakamura, Y. A. Pashkin, T. Yamamoto, and J.-S. Tsai, Charge Echo in a Cooper-Pair Box, *Phys. Rev. Lett.* **88**, 047901 (2002).
- [19] A. I. Nesterov and G. P. Berman, Modeling of low-and high-frequency noise by slow and fast fluctuators, *Phys. Rev. A* **85**, 052125 (2012).
- [20] T. Fujisawa and Y. Hirayama, Charge noise analysis of an AlGaAs/GaAs quantum dot using transmission-type radio-frequency single-electron transistor technique, *Appl. Phys. Lett.* **77**, 543 (2000).
- [21] G. Zimmerli, T. M. Eiles, R. L. Kautz, and J. M. Martinis, Noise in the Coulomb blockade electrometer, *Appl. Phys. Lett.* **61**, 237 (1992).
- [22] L. Faoro and L. B. Ioffe, Quantum Two Level Systems and Kondo-Like Traps as Possible Sources of Decoherence in Superconducting Qubits, *Phys. Rev. Lett.* **96**, 047001 (2006).
- [23] T. Chasseur, L. S. Theis, Y. R. Sanders, D. J. Egger, and F. K. Wilhelm, Engineering adiabaticity at an avoided crossing with optimal control, *Phys. Rev. A* **91**, 043421 (2015).
- [24] J. Bylander, S. Gustavsson, F. Yan, F. Yoshihara, K. Harrabi, G. Fitch, D. G. Cory, Y. Nakamura, J.-S. Tsai, and W. D. Oliver, Noise spectroscopy through dynamical decoupling with a superconducting flux qubit, *Nat. Phys.* **7**, 565 (2011).
- [25] M. Gong, M.-C. Chen, Y. Zheng, S. Wang, C. Zha, H. Deng, Z. Yan, H. Rong, Y. Wu, S. Li *et al.*, Genuine 12-Qubit Entanglement on a Superconducting Quantum Processor, *Phys. Rev. Lett.* **122**, 110501 (2019).
- [26] C. Neill, P. Roushan, K. Kechedzhi, S. Boixo, S. V. Isakov, V. Smelyanskiy, A. Megrant, B. Chiaro, A. Dunsworth, K. Arya *et al.*, A blueprint for demonstrating quantum supremacy with superconducting qubits, *Science* **360**, 195 (2018).
- [27] S. Sheldon, L. S. Bishop, E. Magesan, S. Filipp, J. M. Chow, and J. M. Gambetta, Characterizing errors on qubit operations via iterative randomized benchmarking, *Phys. Rev. A* **93**, 012301 (2016).
- [28] A. Di Paolo, A. L. Grimsmo, P. Groszkowski, J. Koch, and A. Blais, Control and coherence time enhancement of the  $0-\pi$  qubit, *New J. Phys.* **21**, 043002 (2019).
- [29] L. B. Nguyen, Y.-H. Lin, A. Somoroff, R. Mencia, N. Grabon, and V. E. Manucharyan, High-Coherence Fluxonium Qubit, *Phys. Rev. X* **9**, 041041 (2019).
- [30] V. E. Manucharyan, J. Koch, L. I. Glazman, and M. H. Devoret, Fluxonium: Single cooper-pair circuit free of charge offsets, *Science* **326**, 113 (2009).
- [31] Y.-H. Lin, L. B. Nguyen, N. Grabon, J. San Miguel, N. Pankratova, and V. E. Manucharyan, Demonstration of Protection of a Superconducting Qubit from Energy Decay, *Phys. Rev. Lett.* **120**, 150503 (2018).